
Concentration bounds for linear Monge mapping estimation and optimal transport domain adaptation

Rémi Flamary*
Université Côte d'Azur
Lagrange, CNRS, OCA

Karim Lounici*
CMAP, École polytechnique
Université Côte d'Azur

André Ferrari
Université Côte d'Azur
Lagrange, CNRS, OCA

Abstract

This article investigates the quality of the estimator of the linear Monge mapping between distributions. We provide the first concentration result on the linear mapping operator and prove a sample complexity of $n^{-1/2}$ when using empirical estimates of first and second order moments. This result is then used to derive a generalization bound for domain adaptation with optimal transport. As a consequence, this method approaches the performance of theoretical Bayes predictor under mild conditions on the covariance structure of the problem. We also discuss the computational complexity of the linear mapping estimation and show that when the source and target are stationary the mapping is a convolution that can be estimated very efficiently using fast Fourier transforms. Numerical experiments reproduce the behavior of the proven bounds on simulated and real data for mapping estimation and domain adaptation on images.

1 Introduction

Optimal transport (OT) and the related Wasserstein distance has been widely used in machine learning in recent years [1, 2, 3]. OT tools allow for a geometric comparison of distributions and Wasserstein distance is one of the few divergence that can be applied (and sub-differentiated) on empirical distribution with no need for kernel smoothing as done in MMD [4]. In addition to those nice properties, the rising interest of the machine learning community has been possible thanks to the recent development of efficient optimization techniques. For instance entropic regularization [5, 6] has lead to new efficient algorithms that can scale to large datasets and even opened the door to stochastic optimization [7, 8].

Among recent applications of OT, one can cite training of Generative Adversarial Networks, that is a particularly difficult optimization problem, where the Wasserstein distance has been used to provide meaningful gradients [1, 9, 10]. But OT has also been used in other learning problems such as unsupervised Domain Adaptation (DA) that aim at training a classifier that perform well on an unlabeled target dataset using information from a related but different labeled source dataset. Recent works on Optimal Transport for Domain Adaptation (OTDA) have shown that under some assumptions, the optimal transport map [2, 11, 8] (also called Monge map) or the OT matrix itself [12] can be used to transfer label knowledge between the source and target datasets.

While OTDA approaches has been used with success on several DA application, theoretical justifications are still limited. For instance [2] and [13] derived generalization bounds that include a divergence term between the source and target distributions close to that of [14]. Because of this term, those generalization bound require source and target distributions to be similar in order to achieve domain adaptation. Our goal in this paper is to derived explicit generalization bounds for OTDA under milder conditions since OT and its corresponding Monge mapping has the ability to align

*Both authors contributed equally.

distributions. As we will prove it in the following, in order to provide meaningful generalization bounds, the core of our analysis consists in bounding the error of estimation of the empirical Monge mapping.

In this paper we investigate the quality of the estimation of a linear Monge mapping when estimated from empirical distribution with finite number of samples. Concentration bounds have been proved on the value of Wasserstein distance between empirical distributions [15] [16]. Very recent results have investigated the quality of a theoretical estimator that cannot be used in practice and have shown error bounds on the estimated Monge mapping with smoothness conditions of $O(n^{-1/d})$ similar to concentrations of the Wasserstein distance [17]. But this results have several limits, the estimator cannot be computed in practice and the convergence speed is very slow for large dimensionality d .

We focus here on the estimation of a linear Monge mapping that admits in particular a close form solution for transport between Gaussian distribution[18]. We prove that this solution is also the solution for any Borel distributions when the true Monge mapping is linear. Then we obtain the first estimation bounds for the linear Monge mapping based on finite samples of sub-gaussian distributions. This result is then used to derive a new generalization bound for OT Domain Adaptation. We also discuss the numerical complexity of the linear Monge mapping estimation and provide an efficient estimation procedure for stationary signal and image data relying on FFT. This last approach called Convolutional Monge Mapping allows for a fast adaptation of image datasets. Numerical experiments are provided to verify the provided theoretical bounds both in error of the monge mapping and Domain Adaptation generalization.

Definitions In what follows, for any symmetric positive definite matrix B , we denote by $\lambda_{\min}(B)$, $\lambda_{\max}(B)$ the minimum and maximum eigenvalues of B respectively. We also define the effective rank of B by $\mathbf{r}(B) = \frac{\text{tr}(B)}{\lambda_{\max}(B)}$ where $\text{tr}(B)$ is the trace of B . By abuse of notation, $\|\cdot\|$ refers either to the l_2 -norm of a vector or to the operator norm of a matrix. We also define the condition number of B as $\kappa(B) = \frac{\lambda_{\max}(B)}{\lambda_{\min}(B)}$. Finally note that in order to save space we use the binary operators \vee and \wedge to denote maximum and minimum respectively.

2 Linear Monge mapping estimation and concentration

2.1 Linear Monge mapping

Linear Monge mapping between Gaussian distributions Let $\mu_1 = \mathcal{N}(m_1, \Sigma_1)$ and $\mu_2 = \mathcal{N}(m_2, \Sigma_2)$ be two distributions. In the remaining we suppose that both Σ_1 and Σ_2 are symmetric strictly positive definite. The Monge mapping for a quadratic loss between μ_1 and μ_2 can be expressed as

$$T(x) = m_2 + A(x - m_1) \quad (1)$$

with

$$A = \Sigma_1^{-\frac{1}{2}} \left(\Sigma_1^{\frac{1}{2}} \Sigma_2 \Sigma_1^{\frac{1}{2}} \right)^{\frac{1}{2}} \Sigma_1^{-\frac{1}{2}} = A^T \quad (2)$$

This is a well known fact in the Optimal Transport literature [19, 20, 18, 21, 22]. See also [23, Remark 2.29]. Note that as discussed in the supplementary material, the matrix A is actually the matrix geometric mean between Σ_1^{-1} and Σ_2 .

Linear Monge mapping between general distributions The linear mapping between Gaussian distribution discussed above is very elegant but real life data in machine learning seldom follow Gaussian distribution (especially classification problems that are at best a mixture of Gaussian). We now show that even when source and target distribution are not Gaussian, if there exists a positive definite linear mapping between them, then the optimal transport mapping is in fact this linear mapping.

Proposition 1. *Let μ_1 and μ_2 be two Borel probability measures with finite second order moments with expectations m_1, m_2 and positive-definite covariance operators Σ_1, Σ_2 respectively and such that $\mu_2 = \tilde{T}_{\#} \mu_1$ for an affine $\tilde{T}(x) = Bx + c$ with B symmetric positive definite. Then the optimal transport mapping is $T = \tilde{T}$ and is given by Eq. 1-2.*

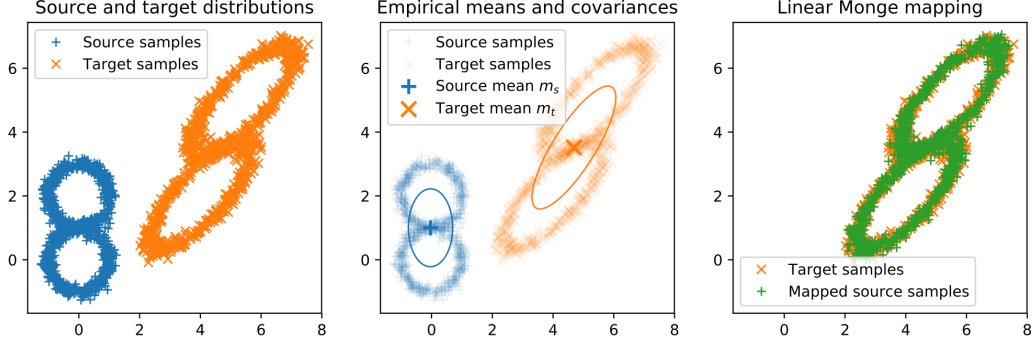


Figure 1: Example of linear Monge mapping estimation between empirical distributions. (left) 2D source and target distributions. (middle) Estimations for means and covariances of the distributions. (right) resulting linear mapping where green samples are the mapped source samples.

Proof. First recall that the Brenier Theorem [24] for quadratic loss states that the optimal transport is the unique map T such that $\mu_2 = T_{\#}\mu_1$ and $T = \nabla\varphi$ for some convex function φ , see [25, Theorem 2.32]. Application of Brenier’s Theorem with $\varphi(x) = (1/2)x^{\top}Bx + c^{\top}x + d$ implies that the optimal transport map T is unique and equal to $T(x) = Bx + c$.

From $\mu_2 = T_{\#}\mu_1$ we know that $m_2 = Bm_1 + c$ and the covariance of the mapped source samples is equal to Σ_2 :

$$B^{\top}\Sigma_1B = \Sigma_2$$

The only symmetric positive definite solution to the Riccati equation above [22, Eq. (8)] is provided by Equation 2. This shows that the linear OT mapping between μ_1 and μ_2 is the same as the one between Gaussians with same covariances. \square

Empirical estimation of the Monge mapping In practice the distributions μ_1, μ_2 are unknown and we have only access to independent samples $\mathbb{X}_1 = \{X_1^s, \dots, X_{n_1}^s\}$ and $\mathbb{X}_2 = \{X_1^t, \dots, X_{n_2}^t\}$ where the X_i^s are i.i.d. with distribution μ_1 and the X_j^t are i.i.d. with distribution μ_2 . In this case, the linear Monge mapping can be estimated using empirical means and covariances $\hat{m}_1, \hat{m}_2, \hat{\Sigma}_1, \hat{\Sigma}_2$ based on n_1 and n_2 samples respectively. Hence we define the empirical linear Monge mapping as

$$\hat{T}(x) = \hat{T}_{(\mathbb{X}_s, \mathbb{X}_t)}(x) = \hat{m}_2 + \hat{A}(x - \hat{m}_1), \quad (3)$$

where \hat{A} comes from Eq. 2 where the covariances are replaced by their empirical counterpart. An illustration of this method for a highly non-Gaussian distribution can be seen in Figure 1. We can clearly see here that under the assumptions in Proposition 1, we can recover the Monge mapping and align very well complex distributions.

2.2 Concentration of the expected mapping error

Let T and T' be two mappings, we define the L_2 -divergence between mapped distributions $T_{\#}\mu_1$ and $T'_{\#}\mu_1$ as

$$d(T, T') = \mathbb{E}_{x \sim \mu_1} [\|T(x) - T'(x)\|^2]. \quad (4)$$

In the next theorem, we prove a bound for the error of estimation of T by \hat{T} .

Theorem 1. *Let μ_1 and μ_2 be sub-Gaussian distributions with expectations m_1, m_2 and positive-definite covariance operators Σ_1, Σ_2 respectively. We assume furthermore that*

$$c < \min_{j=1,2} \{\lambda_{\min}(\Sigma_j)\} \leq \max_{j=1,2} \{\lambda_{\max}(\Sigma_j)\} \leq C, \quad (5)$$

for some fixed absolute constants $0 < c \leq C < \infty$. We also assume that

$$n_j \geq Cr(\Sigma_j), \quad j = 1, 2, \quad (6)$$

for some sufficiently large numerical constant $C > 0$.

Then, for any $t > 0$, we have with probability at least $1 - e^{-t} - \frac{1}{n_1}$,

$$d(T, \hat{T}) \leq C' \left(\sqrt{\frac{\mathbf{r}(\Sigma_1)}{n_1}} \vee \sqrt{\frac{\mathbf{r}(\Sigma_2)}{n_2}} \vee \sqrt{\frac{t}{n_1 \wedge n_2}} \vee \frac{t}{n_1 \wedge n_2} \right) \sqrt{\mathbf{r}(\Sigma_1)}, \quad (7)$$

where $C' > 0$ is a constant independent of $n_1, n_2, \mathbf{r}(\Sigma_1), \mathbf{r}(\Sigma_2)$.

The detailed proof is provided in supplementary material. This result is one of the first bound on the quality of an estimated continuous Monge mapping from empirical distribution. The fact that we limit ourselves to linear Monge mapping means that we can recover a sample complexity of $O(n^{-1/2})$ when $n = n_1 = n_2$ which compares favorably to the $O(n^{-\frac{1}{d}})$ obtained with the more general but not computationally feasible estimator in [17]. Note that this result also provides a convergence rate for the generalization bound in [11, Eq. (13)] in the linear case where the term $d(T, \hat{T})$ appeared in the bound but was not studied.

2.3 Numerical implementation and computational complexity

General covariance matrices The mapping is estimated from empirical distributions by using the empirical version of the means and covariances in Equations (1)-(2). The complexity of estimating those parameters in $O((n_1 + n_2)d^2)$ which is linear *wrt* the number of samples but quadratic in dimensionality d of the data. Equation (2) also requires the commutation of matrix square root and inverse which are $O(d^3)$ leading to a final complexity of $O((n_1 + n_2)d^2 + d^3)$. This complexity scales well with the number of training samples but not with the dimensionality of the space.

Convolutional Monge mapping on signals and images When the data samples are temporally or spatially stationary signal or images, it is a common practice for large d to approximate their Toeplitz or block-Toeplitz covariance matrices by circulant matrices and assume that they are diagonalizable by a discrete Fourier transform: $\Sigma_1 = F\Lambda_1 F^H, \Sigma_2 = F\Lambda_2 F^H$, [26]. In this case the linear operator in (2) is actually a convolution operator with frequency response $D = \Lambda_2^{\frac{1}{2}} \Lambda_1^{-\frac{1}{2}}$:

$$A = FDF^H \quad (8)$$

that can be computed efficiently in the Fourier domain using the Fast Fourier transform (FFT) algorithm. The speedup of the FFT leads to a final computational cost of $O((n_1 + n_2)d \log(d))$ to estimate D that is greatly reduced compared to the general linear case discussed above. Note that in this case in order to use the FFT we suppose that the linear mapping operator is a positive definite circular convolution operator which can introduce artefacts at the border of images.

Regularization We suppose in all our theoretical results that the empirical covariance matrices are strictly positive definite. While this is often true when $n_1 > d$ and $n_2 > d$, in practice this assumption can be false on real data (especially when the data lies in a linear sub-manifold). A classical practice is to replace the empirical covariance matrix Σ_i by $\tilde{\Sigma}_i = (1 - \alpha)\Sigma_i + \alpha I$ where $\alpha \geq 0$ and I is the identity matrix. In our numerical experiments we did not use this regularization in the simulated examples but needed to use it with a small $\alpha = 10^{-6}$ on the real life image data.

3 Domain adaptation generalization bound

Now we focus on the problem of domain adaptation where we have access to data from a source joint feature/label distribution \mathcal{P}_s but want to predict well on a target joint distribution \mathcal{P}_t where only features are available (the marginal distribution μ_t). We define the risk of a prediction rule f in the source domain as

$$R_s(f) := \mathbb{E}_{(x,y) \sim \mathcal{P}_s} [L(y, f(x))]. \quad (9)$$

where L is a loss of Lipschitz constant M_L *wrt* its second variable. For instance we have $M_L = 1$ for SVM Hinge loss for instance independently of the class y . The risk on the target domain $R_t(f)$ is

defined similarly with an expectation done wrt \mathcal{P}_t . The optimal prediction rule on the source domain is defined as

$$f_*^s := \operatorname{argmin}_{f: \mathbb{R}^d \rightarrow \mathbb{R}} R_s(f), \quad (10)$$

where the minimization is taken over all measurable functions. We assume here for simplicity that the minimum is attained. Similarly the optimal prediction rule on target is defined as f_*^t .

Optimal Transport Domain Adaptation One major assumption that was made in [2] is that there exist a mapping m between the source and target such that $\mathcal{P}_t = m_{\#}\mathcal{P}_s$ and that the pushforward m can be expressed as $m(x, y) = (T(x), y)$. In other words the samples in the feature space have been transformed by T but have conserved their label through this transformation. This assumption corresponds to a number of real life situations such as a change in the acquisition conditions, sensor drifts, thermal noise in signal processing. This implies that for functions f and g in the source and target domains respectively :

$$R_s(f) = R_t(f \circ T^{-1}) \quad \text{and} \quad R_t(g) = R_s(g \circ T) \quad (11)$$

where T is assumed to be invertible. Note that (11) and (10) imply that the best performance in the source and target domains are equal $R_s(f_*^s) = R_t(f_*^t)$. This motivated the main idea in [2] that if one can estimate the mapping T , then it is possible to map the labeled source samples in the target domain with \hat{T} and train a classifier \hat{g} in the target domain using the labels from the original source samples. This classifier can predict the labels for new data in the target domain. In the following we investigate the generalization performance of a similar procedure where we train a classifier \hat{f} in the source domain and use $\hat{f} \circ \hat{T}^{-1}$ to predict in the target domain.

Generalization bound Ideally, the goal is to build a prediction rule g that performs almost as well as the optimal prediction rule in the target domain w.r.t. the generalization error $R_t(g)$. Without available labels in the target domain this goal seems out of reach as illustrated by the impossibility theorem in [14]. But our assumption that a mapping T exists can be used to find a good prediction rule. In view of (11), if f is a prediction rule in the source domain, then $g = f \circ T^{-1}$ is a prediction rule in the target domain such that $R_t(g) = R_s(f)$. Since T is unknown, we replace it by an estimator \hat{T} as defined in (3).

Theorem 2. *Let f be a prediction rule in the source domain with a Lipschitz constant M_f and R_p the expected risk on domain p with a Lipschitz continuous loss L of constant M_L . Under the OTDA assumptions (11) we have the following generalization bound*

$$R_t(f \circ \hat{T}^{-1}) \leq R_s(f) + M_f M_L \mathbb{E}_{(x,y) \sim \mathcal{P}_s} \left[\|\hat{T}^{-1}(T(x)) - \hat{T}^{-1}(\hat{T}(x))\| \right] \quad (12)$$

If \hat{T} is the linear mapping as defined in (3) then we have

$$R_t(f \circ \hat{T}^{-1}) \leq R_s(f) + M_f M_L \|\hat{A}^{-1}\| d(T, \hat{T}) \quad (13)$$

This result means that our estimated transferred rule $f \circ \hat{T}^{-1}$ will perform almost as well in the target domain as the initial rule f in the source domain up to a remainder term that depends on the transport mapping. Note that (30) is valid for arbitrary transport while (31) is specific to linear Monge mapping.

Generalization bound for finite samples Note that our goal is to learn a good prediction rule in the target domain $\hat{f} : \mathbb{R}^d \rightarrow T$ from finite datasets. To this end we have access to respectively n_1 and n_2 unlabeled samples in $\mathbb{X}_s, \mathbb{X}_t$ from the source and target domains that will be used to estimate the mapping \hat{T} . We also have access to n_l labeled samples (X_i^l, Y_i^l) , $i = 1, \dots, n_l$ in the source domain independently samples from \mathbb{X}_s .

Theorem 3. *Let \mathcal{H}_K be a reproducing kernel Hilbert space (RKHS) associated with a symmetric nonnegatively definite kernel $K : \mathbb{R}^d \times \mathbb{R}^d \rightarrow \mathbb{R}$ such that for any $x \in \mathbb{R}^d$, $K_x(\cdot) = K(\cdot, x) \in \mathcal{H}_K$ and $f(x) = \langle f(x), K_x \rangle_{\mathcal{H}_K}$ for all $f \in \mathcal{H}_K$. Assume that $f_* \in \mathcal{H}_K$ and $\|f_*\|_{\mathcal{H}_K} \leq 1$. We consider the following empirical risk minimization estimator:*

$$\hat{f}_{n_l} := \operatorname{argmin}_{\|f\|_{\mathcal{H}_K} \leq 1} \frac{1}{n_l} \sum_{i=1}^{n_l} l(Y_i^l, f(X_i^l)). \quad (14)$$

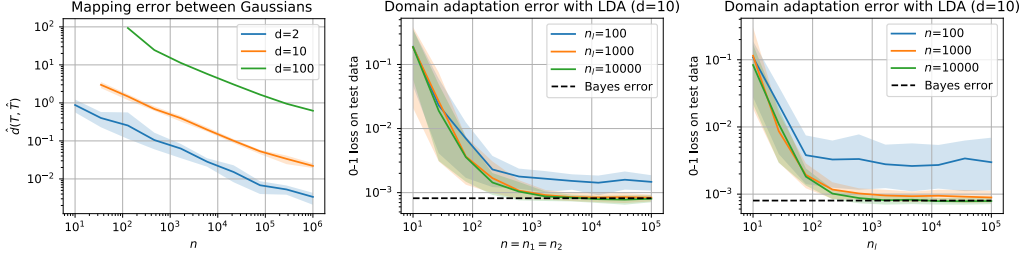


Figure 2: Experiments with Gaussian data. (left) mapping error as a function of $n = n_1 = n_2$ for different values of d (left) domain adaptation test error rate as a function of n (right) domain adaptation test error rate as a function of n_l . Colored area corresponds to 10th and 90th percentile.

where we assume that the eigenvalues of the integral operator T_K of \mathcal{H}_K decrease with $\lambda_k \asymp k^{-2\beta}$ for some $\beta > 1/2$ (see [27]). If $R_s(f_*^s) = R_t(f_*^t)$ and \hat{T} is the linear mapping as defined in (3), under the assumptions of Theorem 1, we get with probability at least $1 - e^{-t} - \frac{1}{n_1}$,

$$R_t(\hat{f}_{n_l} \circ \hat{T}^{-1}) - R_t(f_*^t) \lesssim n_l^{-2\beta/(1+2\beta)} + \frac{t}{n_l} \quad (15)$$

$$+ M_f M_L \left(\sqrt{\frac{\mathbf{r}(\Sigma_2)}{n_2}} \vee \sqrt{\frac{\mathbf{r}(\Sigma_1)}{n_1}} \vee \sqrt{\frac{t}{n_1 \wedge n_2}} \vee \frac{t}{n_1 \wedge n_2} \right) \sqrt{\mathbf{r}(\Sigma_1)}.$$

The proof of the previous theorem and more details about the assumptions in the RKHS are available in supplementary. The bound above prove that under the mapping assumption, the generalization error of $\hat{f}_{n_l} \circ \hat{T}^{-1}$ converges to the Bayes risk $R_t(f_*^t)$ in the target domain even though we do not have access to target labels during the training phase. This is to the best of our knowledge the first theoretical result that leads to such performances on unsupervised domain adaptation problem. We can get away from the impossibility theorem of domain adaptation of [14] thanks to the strong assumption on the existence of a linear Monge mapping that allows reducing the distribution discrepancy with the mapping. Finally note that while this result is specific to linear Monge mapping, it can be easily extended to any mapping estimation such as Virtual Regressive training [28] that also have a $o(n^{-1/2})$ convergence speed when n is the number of one-to-one mapping samples between source and target domain.

4 Numerical experiments

In this section we provide numerical experiments that aim at verifying our theoretical results. The linear mapping estimation from (3) is implemented using class `LinearTransport` from the Python Optimal Transport library [29].

4.1 Convergence of the mapping error and domain adaptation generalization

Linear mapping error between Gaussian distributions In a first numerical experiments we illustrate the convergence speed in term of mapping quality as a function of the number of samples in source and target domains $n = n_1 = n_2$. To this end, for every dimensionality d we generate Gaussian distributions with random means $\mu_i \sim \mathcal{N}(\mathbf{0}, 10I_d)$ and covariance $\Sigma_i \sim \mathcal{W}_d(I, d)$ following Wishart distributions of order d . For each (μ_i, Σ_i) we generate $n = n_1 = n_2$ Gaussian distributed samples.

All experiments are repeated 10 times (Monte Carlo) and the mean mapping error is computed on 10^6 source samples. Figure 2(left) shows the convergence in n for different values of dimensionality d . This log/log plot clearly shows the slope of $-\frac{1}{2}$ corresponding to the $O(n^{-\frac{1}{2}})$ convergence speed in Theorem 1.

Domain adaptation of simulated examples Next we reproduce the domain adaptation bounds discussed in section 3. To this end we design a classification problem where samples from class + are

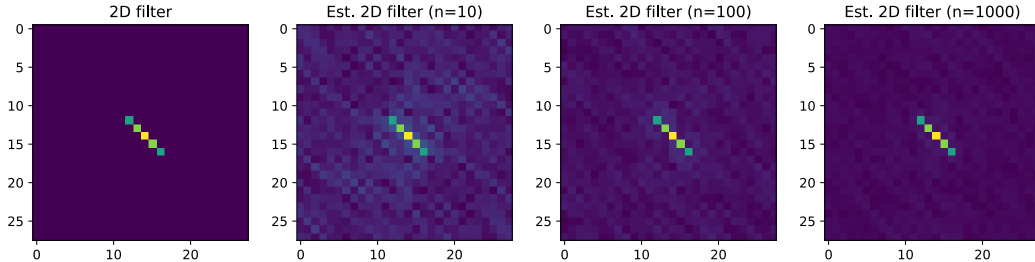


Figure 3: (left) 2D motion blur filter applied to the target MNIST images. (center to right) estimated 2D filters for different number of samples $n = n_1 = n_2$ for the filter estimation. All images are shown with a square root of their magnitude in order to better see small errors.

drawn from $\mathcal{N}(\mathbf{0}, \Sigma_0)$ and samples from class - from $\mathcal{N}(\mathbf{1}, \Sigma_0)$, which can be solved with the LDA linear classifier. We draw a linear mapping $T(x) = Bx + c$ where the operator B is a realization of a Wishart distribution of order d and the bias term is a vector $c = [10, 10, \dots, 0, 0]$ with half of its values set to 10 and 0 elsewhere (so that training on source data leads to very bad performance on target). All numerical experiments were performed with $d = 10$. The number of training samples in the source domain is denoted as n_l and the number of unlabeled samples in source and target is $n = n_1 = n_2$ as in the previous experiments.

We estimate the mapping \hat{T}^{-1} from n sample and the classifier \hat{f}_{n_l} in the source domain from n_l independent labeled samples as suggested by Eq. 15. The average classification error rate on 50 Monte Carlo realizations is reported in Figure 2(center) and (right) for different values of n and n_l respectively. We can see in both plots that when both n and n_l become large, the error rate converges to the Bayes error rate $R_t(f_*^t)$ since the problem is not perfectly separable.

4.2 Convolutional Monge mapping between images

In this section we investigate the estimation of Monge mapping between images when the mapping is a convolution. To this end we use the well known MNIST dataset [30] for both 2D filter estimation and convolutional domain adaptation.

2D Filter estimation between distributions In order to see if our approach is able to recover a convolution operator between two datasets, we design a simple positive definite motion blur filtering illustrated in Figure 3 (left), that is used to generate the target images from original MNIST images. Example images from the source distribution (original MNIST) can be seen at the top line of Figure 4 and examples from the target distribution (filtered MNIST) can be seen at the bottom. Note that the source and target (filtered source) samples do not overlap in all the numerical experiments.

The 2D filters estimated using Eq. 8 for a different number of samples in source/target can be seen in the right part of Figure 3. Note that even for $n = 10$ the filter is surprisingly well estimated considering that there is not even one sample per class in the source/target distributions. For $n = 1000$ the error on the filter is not visible anymore which is also very good for a problem of dimensionality $d = 28 \times 28 = 784$ variables (pixels). We provide also a visualization of the source samples from the top line of Figure 4 after convolution by the estimated filter in the center line of the Figure and we can see that the mapped samples are very similar to the target samples.

In order to have a quantitative measure of the quality of both linear and convolutional Monge mapping we perform 20 monte Carlo experiments where we randomly draw a varying number of n samples for estimating the filter described above. The mapping for the linear Monge mapping is estimated using the general formulation in Eq. 3 whereas for convolutional mapping, we use the simplified formulation in Eq. 8 computed by FFT. The average error of the mapping for both approaches is reported in Figure 5(left). We can see that the linear mapping has a hard time estimating the mapping especially when $n < d$ (estimated covariance matrix is singular but small regularization is used) but recovers its theoretical convergence speed for $n \geq 10^3$. The convolutional mapping that is much more structured and estimates a smaller number of parameter (block Toeplitz covariance matrix) shows its theoretical convergence speed for $n \geq 10$.

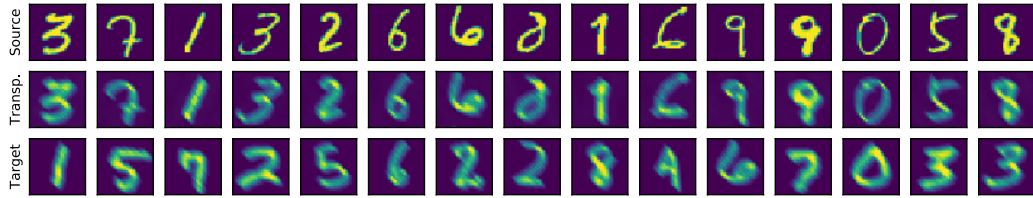


Figure 4: Example images from the MNIST images data. (top) Images from the source distribution. (middle) Examples from the source distribution mapped to the target distribution (convolved with estimated filter). (bottom) Examples from the Target distribution (with the motion blur filter applied).

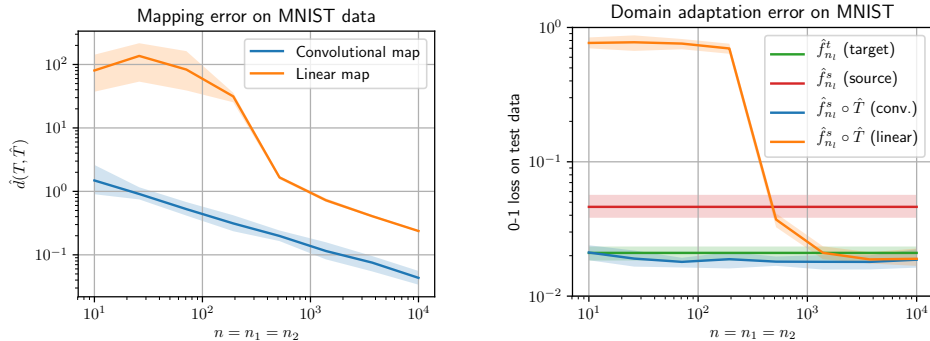


Figure 5: (left) Mapping error on the MNIST data for a convolutional and linear mapping (right) Target prediction error for domain adaptation problem with training on source, training on target and OTDA with linear and convolutional mapping.

Convolutional mapping for domain adaptation We then investigate the performance in domain adaptation between the two domains presented above (from original to filtered MNIST) when training a Convolutional Neural Network (CNN) in the source domain. We use the architecture from the MNIST example of Keras² with all hyperparameters fixed (nb epoch, step, minibatch) for all comparisons. CNN are trained on $n_l = 10^4$ samples and their test error rate is evaluated also on 10^4 independent target samples. We first compute baselines with a CNN trained on source domain ($\hat{f}_{n_l}^s$) and target domain ($\hat{f}_{n_l}^t$). This last approach is not domain adaptation since some labeled target data is available to train a classifier but provides a reasonable performance on target for comparison. We also compare the performance of OTDA with classifier $\hat{f}_{n_l}^s \circ \hat{T}^{-1}$ when \hat{T} is estimated using Linear (linear) and Convolutional (conv.) Monge Mapping estimation. The average classification error on test over 20 Monte Carlo simulations (data sampling) with a varying $n = n_1 = n_2$ is reported in Figure 5(right). We can see that the convolutional mapping quickly reaches the performance of classifier $\hat{f}_{n_l}^t$ trained directly on target data. This might be due to a regularization effect coming from the convolution operator \hat{T}^{-1} to the data before classification that also seem to lead to a slightly better final performance than $\hat{f}_{n_l}^t$. The linear Monge mapping requires more samples for a proper mapping ($n \geq 10^3$) estimation but also reaches the best performance on target.

5 Conclusion

In this work, we provided the first concentration bound on the quality of a linear Monge mapping when estimated from a discrete sampling. We have shown that this linear mapping can be estimated from non-Gaussian distributions. We discussed the computational complexity of the linear Monge mapping estimation and investigated a variant that leads to both a speedup and better estimation when the data is a 1D/2D stationary signal which implies a convolutional mapping. This fundamental results allowed us to prove the first bound for Optimal Transport Domain Adaptation [2] that actually

²Available at https://github.com/keras-team/keras/blob/master/examples/mnist_cnn.py

converge to the Bayes risk for large number of samples. Finally we provided numerical experiments that recover the theoretical bounds for both linear and convolutional mapping.

Future works will investigate the design and convergence of an applicable non-linear Monge mapping estimated from finite distributions [17]. An approach would be to study the quality of the barycentric mapping that has been used in practice [31, 2] and is known to converge weakly to the true Monge mapping [8]. The study of the mapping estimation in the presence of additive noise is also an interesting research direction related to Gaussian deconvolution [32]. Also note that the estimation of a convolutional mapping between distributions of images opens the door for applications in image processing and especially in astronomy where it could be used to estimate changes in the Point Spread Function (filter) of a telescope or parameters of weak gravitational lensing [33].

Acknowledgements

The authors want to thank Gabriel Peyré and Nicolas Courty for fruitful discussions about linear Monge mapping and domain adaptation. This work benefited from the support from OATMIL ANR-17-CE23-0012 project of the French National Research Agency (ANR).

References

- [1] Martin Arjovsky, Sumit Chintala, and Léon Bottou. Wasserstein generative adversarial networks. In *ICML*, pages 214–223, 2017.
- [2] N. Courty, R. Flamary, D. Tuia, and A. Rakotomamonjy. Optimal transport for domain adaptation. *Pattern Analysis and Machine Intelligence, IEEE Transactions on*, 2017.
- [3] C. Frogner, C. Zhang, H. Mobahi, M. Araya, and T. Poggio. Learning with a Wasserstein loss. In *NIPS*. 2015.
- [4] Arthur Gretton, Karsten M Borgwardt, Malte J Rasch, Bernhard Schölkopf, and Alexander Smola. A kernel two-sample test. *Journal of Machine Learning Research*, 13(Mar):723–773, 2012.
- [5] Marco Cuturi. Sinkhorn distances: Lightspeed computation of optimal transport. In *NIPS*, 2013.
- [6] Jean-David Benamou, Guillaume Carlier, Marco Cuturi, Luca Nenna, and Gabriel Peyré. Iterative bregman projections for regularized transportation problems. *SIAM Journal on Scientific Computing*, 37(2):A1111–A1138, 2015.
- [7] Aude Genevay, Marco Cuturi, Gabriel Peyré, and Francis Bach. Stochastic optimization for large-scale optimal transport. In *Advances in Neural Information Processing Systems*, pages 3440–3448, 2016.
- [8] Vivien Seguy, Bharath B. Damodaran, Remi Flamary, Nicolas Courty, Antoine Rolet, and Mathieu Blondel. Large-scale optimal transport and mapping estimation. In *International Conference on Learning Representations (ICLR)*, 2018.
- [9] Huidong Liu, GU Xianfeng, and Dimitris Samaras. A two-step computation of the exact gan wasserstein distance. In *International Conference on Machine Learning*, pages 3165–3174, 2018.
- [10] Na Lei, Kehua Su, Li Cui, Shing-Tung Yau, and Xianfeng David Gu. A geometric view of optimal transportation and generative model. *Computer Aided Geometric Design*, 68:1–21, 2019.
- [11] Michaël Perrot, Nicolas Courty, Rémi Flamary, and Amaury Habrard. Mapping estimation for discrete optimal transport. In *Advances in Neural Information Processing Systems*, pages 4197–4205, 2016.
- [12] Nicolas Courty, Rémi Flamary, Amaury Habrard, and Alain Rakotomamonjy. Joint distribution optimal transportation for domain adaptation. In *Advances in Neural Information Processing Systems*, pages 3730–3739, 2017.
- [13] Ievgen Redko, Amaury Habrard, and Marc Sebban. Theoretical analysis of domain adaptation with optimal transport. In *Joint European Conference on Machine Learning and Knowledge Discovery in Databases*, pages 737–753. Springer, 2017.

- [14] Shai Ben-David, Tyler Lu, Teresa Luu, and Dávid Pál. Impossibility theorems for domain adaptation. In *International Conference on Artificial Intelligence and Statistics*, pages 129–136, 2010.
- [15] Nicolas Fournier and Arnaud Guillin. On the rate of convergence in wasserstein distance of the empirical measure. *Probability Theory and Related Fields*, 162(3-4):707–738, 2015.
- [16] Jonathan Weed and Francis Bach. Sharp asymptotic and finite-sample rates of convergence of empirical measures in wasserstein distance. *arXiv preprint arXiv:1707.00087*, 2017.
- [17] Jan-Christian Hütter and Philippe Rigollet. Minimax rates of estimation for smooth optimal transport maps. *arXiv preprint arXiv:1905.05828*, 2019.
- [18] Asuka Takatsu et al. Wasserstein geometry of gaussian measures. *Osaka Journal of Mathematics*, 48(4):1005–1026, 2011.
- [19] Clark R Givens, Rae Michael Shortt, et al. A class of wasserstein metrics for probability distributions. *The Michigan Mathematical Journal*, 31(2):231–240, 1984.
- [20] Robert J McCann. A convexity principle for interacting gases. *Advances in mathematics*, 128(1):153–179, 1997.
- [21] Rajendra Bhatia, Tanvi Jain, and Yongdo Lim. On the bures–wasserstein distance between positive definite matrices. *Expositiones Mathematicae*, 2018.
- [22] Luigi Malagò, Luigi Montrucchio, and Giovanni Pistone. Wasserstein riemannian geometry of gaussian densities. *Information Geometry*, 1(2):137–179, 2018.
- [23] Gabriel Peyré, Marco Cuturi, et al. Computational optimal transport. *Foundations and Trends® in Machine Learning*, 11(5-6):355–607, 2019.
- [24] Yann Brenier. Polar factorization and monotone rearrangement of vector-valued functions. *Communications on pure and applied mathematics*, 44(4):375–417, 1991.
- [25] Cédric Villani. *Topics in Optimal Transportation*. American Mathematical Society, March 2003.
- [26] Robert M. Gray. Toeplitz and circulant matrices: A review. *Foundations and Trends® in Communications and Information Theory*, 2(3):155–239, 2005.
- [27] Shahar Mendelson. Geometric parameters of kernel machines. In Jyrki Kivinen and Robert H. Sloan, editors, *Computational Learning Theory*, pages 29–43, Berlin, Heidelberg, 2002. Springer Berlin Heidelberg.
- [28] Michaël Perrot and Amaury Habrard. Regressive virtual metric learning. In *Advances in Neural Information Processing Systems*, pages 1810–1818, 2015.
- [29] Rémi Flamary and Nicolas Courty. Pot: Python optimal transport library, 2017.
- [30] Yann LeCun. The mnist database of handwritten digits. <http://yann.lecun.com/exdb/mnist/>, 1998.
- [31] Sira Ferradans, Nicolas Papadakis, Gabriel Peyré, and Jean-François Aujol. Regularized discrete optimal transport. *SIAM Journal on Imaging Sciences*, 7(3):1853–1882, 2014.
- [32] Philippe Rigollet and Jonathan Weed. Entropic optimal transport is maximum-likelihood deconvolution. *Comptes Rendus Mathématique*, 356(11-12):1228–1235, 2018.
- [33] Dipak Munshi, Patrick Valageas, Ludovic Van Waerbeke, and Alan Heavens. Cosmology with weak lensing surveys. *Physics Reports*, 462(3):67–121, 2008.
- [34] Daniel Hsu, Sham Kakade, and Tong Zhang. A tail inequality for quadratic forms of subgaussian random vectors. *Electron. Commun. Probab.*, 17:6 pp., 2012.
- [35] Bernhard A. Schmitt. Perturbation bounds for matrix square roots and pythagorean sums. *Linear Algebra and its Applications*, 174:215 – 227, 1992.
- [36] Per-Åke Wedin. Perturbation theory for pseudo-inverses. *BIT Numerical Mathematics*, 13(2):217–232, 1973.
- [37] Vladimir Koltchinskii, Karim Lounici, et al. Asymptotics and concentration bounds for bilinear forms of spectral projectors of sample covariance. In *Annales de l’Institut Henri Poincaré, Probabilités et Statistiques*, volume 52, pages 1976–2013. Institut Henri Poincaré, 2016.
- [38] N. Aronszajn. Theory of reproducing kernels. *Transactions of the American Mathematical Society*, 68:337–404, 1950.

Supplementary material

6 Proof of Theorem 1

From now on, by abuse of notation, $\|\cdot\|$ will refer either to the l_2 -norm of a vector or the operator norm of a matrix.

We first observe that

$$\begin{aligned} \|T(x) - \hat{T}(x)\| &= \|m_2 - \hat{m}_2 + (A - \hat{A})(x - m_1 + \hat{A}(m_1 - \hat{m}_1))\| \\ &\leq \|m_2 - \hat{m}_2\| + \|A - \hat{A}\| \|x - m_1\| + \|\hat{A}\| \|\hat{m}_1 - m_1\|. \end{aligned} \quad (16)$$

6.1 Bounding $\|\hat{m}_j - m_j\|$, $j = 1, 2$.

Bounding $\|\hat{m}_j - m_j\|$, $j = 1, 2$ poses no particular difficulty. We have $X^s \stackrel{d}{=} \Sigma_1^{1/2} Z$ where $Z \in \mathbb{R}^p$ is a sub-Gaussian random vector, that is, for any deterministic vector α , we have

$$\mathbb{E}[\exp(\langle \alpha, Z_i \rangle)] \leq \exp\left(\frac{\|\alpha\|^2}{2}\right).$$

Note that

$$\hat{m}_1 - m_1 \stackrel{d}{=} \Sigma_1^{1/2} \frac{1}{n_1} \sum_{i=1}^{n_1} Z_i,$$

where Z_1, \dots, Z_{n_1} are independent distributed as Z . Theorem 2.1 in [34] gives for any $t > 0$, with probability at least $1 - e^{-t}$,

$$\|\hat{m}_1 - m_1\|^2 \leq \frac{\|\Sigma_1\|}{n_1} \left[\mathbf{r}(\Sigma_1) + 2\sqrt{\mathbf{r}(\Sigma_1)t} + 2t \right] \quad (17)$$

A similar bound holds valid for X^t with Σ_1 and n_1 replaced by Σ_2 and n_2 .

6.2 Bounding $\|A - \hat{A}\|$

We concentrate now on $\|A - \hat{A}\|$ that requires more work. We prove the following result.

Theorem 4. *Let μ_1 and μ_2 be sub-Gaussian distributions with respective means and covariance μ_j, Σ_j , $j = 1, 2$. Assume that*

$$C \left(\sqrt{\frac{\mathbf{r}(\Sigma_1)}{n_1}} \vee \frac{\mathbf{r}(\Sigma_1)}{n_1} \vee \sqrt{\frac{\log(n_1)}{n_1}} \right) \leq \frac{1}{2} \min \left\{ \frac{1}{\kappa(\Sigma_1)}, 1, \frac{\lambda_{\min}(\Sigma_2 \Sigma_1)}{\|\Sigma_1\| \|\Sigma_2\|} \right\}, \quad (18)$$

for some sufficiently large numerical constant $C > 0$. Then we have with probability at least $1 - e^{-t} - \frac{1}{n_1}$,

$$\begin{aligned} \|\hat{A} - A\| &\lesssim \frac{\kappa(\Sigma_1) \|\Sigma_2\|}{\lambda_{\min}^{1/2}(\Sigma_1 \Sigma_2)} \left(\sqrt{\frac{\mathbf{r}(\Sigma_2)}{n_2}} \vee \frac{\mathbf{r}(\Sigma_2)}{n_2} \vee \sqrt{\frac{t}{n_2}} \vee \frac{t}{n_2} \right) \\ &\quad + \frac{\kappa(\Sigma_2) \kappa(\Sigma_1) \|\Sigma_2\|}{\lambda_{\min}^{1/2}(\Sigma_2^{-1} \Sigma_1)} \left(\sqrt{\frac{\mathbf{r}(\Sigma_1)}{n_1}} \vee \frac{\mathbf{r}(\Sigma_1)}{n_1} \vee \sqrt{\frac{\log n_1}{n_1}} \right). \end{aligned} \quad (19)$$

Matrix geometric mean. We recall first some useful facts. The geometric mean of 2 positive definite matrices is defined as

$$B \# C := B^{1/2} (B^{-1/2} C B^{-1/2})^{1/2} B^{1/2} = B (B^{-1} C)^{1/2}.$$

Note that for readability, in the remaining of this section, the $\#$ operator refers to the matrix geometric mean and not to the pushforward operator $\#$ used in the main paper. The matrix geometric mean satisfies

$$\begin{aligned} B \# C &= C \# B \\ (B \# C)^{-1} &= B^{-1} \# C^{-1}. \end{aligned}$$

Based on the last two displays, we deduce that

$$\begin{aligned}
\hat{A} - A &= \hat{\Sigma}_1^{-1} \# \hat{\Sigma}_2 - \Sigma_1^{-1} \# \Sigma_2 \\
&= \hat{\Sigma}_1^{-1} \# \hat{\Sigma}_2 - \hat{\Sigma}_1^{-1} \# \Sigma_2 + \hat{\Sigma}_1^{-1} \# \Sigma_2 - \Sigma_1^{-1} \# \Sigma_2 \\
&= \hat{\Sigma}_1^{-1} \# \hat{\Sigma}_2 - \hat{\Sigma}_1^{-1} \# \Sigma_2 + \Sigma_2 \# \hat{\Sigma}_1^{-1} - \Sigma_2 \# \Sigma_1^{-1} \\
&= \hat{\Sigma}_1^{-1} \# \hat{\Sigma}_2 - \hat{\Sigma}_1^{-1} \# \Sigma_2 + (\Sigma_2^{-1} \# \hat{\Sigma}_1)^{-1} - (\Sigma_2^{-1} \# \Sigma_1)^{-1}.
\end{aligned} \tag{20}$$

Next we have by definition of the matrix geometric mean that

$$\hat{\Sigma}_1^{-1} \# \hat{\Sigma}_2 - \hat{\Sigma}_1^{-1} \# \Sigma_2 = \hat{\Sigma}_1^{-1/2} \left[(\hat{\Sigma}_1^{1/2} \hat{\Sigma}_2 \hat{\Sigma}_1^{1/2})^{1/2} - (\hat{\Sigma}_1^{1/2} \Sigma_2 \hat{\Sigma}_1^{1/2})^{1/2} \right] \hat{\Sigma}_1^{-1/2}.$$

Taking the operator norm, we get

$$\|\hat{\Sigma}_1^{-1} \# \hat{\Sigma}_2 - \hat{\Sigma}_1^{-1} \# \Sigma_2\| \leq \|\hat{\Sigma}_1^{-1/2}\|^2 \|(\hat{\Sigma}_1^{1/2} \hat{\Sigma}_2 \hat{\Sigma}_1^{1/2})^{1/2} - (\hat{\Sigma}_1^{1/2} \Sigma_2 \hat{\Sigma}_1^{1/2})^{1/2}\|.$$

Perturbation argument. We set $B = \hat{\Sigma}_1^{\frac{1}{2}} \Sigma_2 \hat{\Sigma}_1^{\frac{1}{2}}$ and $\hat{B} = \hat{\Sigma}_1^{\frac{1}{2}} \hat{\Sigma}_2 \hat{\Sigma}_1^{\frac{1}{2}}$. Note that $X = \hat{B}^{1/2} - B^{1/2}$ is solution of $XU + VX = W$, with $U = \hat{B}^{1/2}$, $V = B^{1/2}$, $W = \hat{B} - B$. Then, we can apply Lemma 2.1 in [35] to obtain the following bound:

$$\|X\| \leq \frac{1}{\lambda_{\min}(B^{1/2})} \|\hat{B} - B\|. \tag{21}$$

where $\lambda_{\min}(A)$ is the minimum eigenvalue of symmetric matrix A .

Thus we get

$$\|X\| \leq \frac{1}{\lambda_{\min}(B^{1/2})} \|\hat{\Sigma}_1\| \|\hat{\Sigma}_2 - \Sigma_2\|.$$

Combining the previous display with (21), we deduce that

$$\|\hat{\Sigma}_1^{-1} \# \hat{\Sigma}_2 - \hat{\Sigma}_1^{-1} \# \Sigma_2\| \leq \frac{\kappa(\hat{\Sigma}_1)}{\lambda_{\min}((\hat{\Sigma}_1^{\frac{1}{2}} \Sigma_2 \hat{\Sigma}_1^{\frac{1}{2}})^{1/2})} \|\hat{\Sigma}_2 - \Sigma_2\|, \tag{22}$$

where $\kappa(A) = \|A^{-1}\| \|A\|$ is the condition number of A .

We study now the second difference in the right-hand side of (20). In view of [36], we have

$$\|(\Sigma_2^{-1} \# \hat{\Sigma}_1)^{-1} - (\Sigma_2^{-1} \# \Sigma_1)^{-1}\| \leq \|(\Sigma_2^{-1} \# \hat{\Sigma}_1)^{-1}\| \|(\Sigma_2^{-1} \# \Sigma_1)^{-1}\| \|\Sigma_2^{-1} \# \hat{\Sigma}_1 - \Sigma_2^{-1} \# \Sigma_1\|.$$

A similar reasoning to that yielding (22) gives us

$$\|\Sigma_2^{-1} \# \hat{\Sigma}_1 - \Sigma_2^{-1} \# \Sigma_1\| \leq \frac{\kappa(\Sigma_2) \|\Sigma_2 \# \hat{\Sigma}_1^{-1}\| \|\Sigma_2 \# \Sigma_1^{-1}\|}{\lambda_{\min}((\Sigma_2^{-1/2} \Sigma_1 \Sigma_2^{-1/2})^{1/2})} \|\hat{\Sigma}_1 - \Sigma_1\|. \tag{23}$$

Combining the last display with (20) and (22), we obtain

$$\|\hat{A} - A\| \leq \frac{\kappa(\hat{\Sigma}_1)}{\lambda_{\min}(\hat{\Sigma}_1^{\frac{1}{2}} \Sigma_2 \hat{\Sigma}_1^{\frac{1}{2}})} \|E_2\| + \frac{\kappa(\Sigma_2) \|\Sigma_2 \# \hat{\Sigma}_1^{-1}\| \|\Sigma_2 \# \Sigma_1^{-1}\|}{\lambda_{\min}(\Sigma_2^{-1/2} \Sigma_1 \Sigma_2^{-1/2})} \|E_1\|. \tag{24}$$

with $E_1 := \hat{\Sigma}_1 - \Sigma_1$ and $E_2 := \hat{\Sigma}_2 - \Sigma_2$.

We now need to control the following random terms: $\kappa(\hat{\Sigma}_1)$, $\lambda_{\min}((\hat{\Sigma}_1^{\frac{1}{2}} \Sigma_2 \hat{\Sigma}_1^{\frac{1}{2}})^{1/2})$ and $\|\Sigma_2 \# \hat{\Sigma}_1^{-1}\|$. To this end, we introduce the event

$$\mathcal{E}_1 = \left\{ \|\Sigma_1^{-1} E_1\| \leq \frac{1}{2} \right\} \cap \left\{ \|E_1\| \leq \frac{\|\Sigma_1\|}{2} \right\} \cap \left\{ \|E_1\| \leq \frac{\lambda_{\min}(\Sigma_2 \Sigma_1)}{2 \|\Sigma_2\|} \right\}. \tag{25}$$

We have on \mathcal{E}_1 that

$$\|\hat{\Sigma}_1^{-1} - \Sigma_1^{-1}\| \leq 2 \|\Sigma_1^{-1} E_1\| \|\Sigma_1^{-1}\|,$$

and consequently

$$\|\hat{\Sigma}_1^{-1}\| \leq 2\|\Sigma_1^{-1}\|, \quad \|\hat{\Sigma}_1\| \leq \frac{3}{2}\|\Sigma_1\|.$$

Thus we have on \mathcal{E}_1 that

$$\kappa(\hat{\Sigma}_1) \leq 3\kappa(\Sigma_1)$$

and

$$\|\Sigma_2 \# \hat{\Sigma}_1^{-1}\| \leq \|\Sigma_2\|^{1/2} \|\hat{\Sigma}_1^{-1}\|^{1/2} \leq \sqrt{2} \|\Sigma_2\|^{1/2} \|\Sigma_1^{-1}\|^{1/2}.$$

Next, applying again Lemma 2.1 in [35], we get that

$$\left| \lambda_{\min}((\hat{\Sigma}_1^{1/2} \Sigma_2 \hat{\Sigma}_1^{1/2})^{1/2}) - \lambda_{\min}((\Sigma_1^{1/2} \Sigma_2 \Sigma_1^{1/2})^{1/2}) \right| \leq \frac{1}{\lambda_{\min}^{1/2}(\Sigma_2 \Sigma_1)} \|\Sigma_2 E_1\|.$$

Thus, we get on the event \mathcal{E}_1 that

$$\lambda_{\min}^{1/2}(\hat{\Sigma}_1^{1/2} \Sigma_2 \hat{\Sigma}_1^{1/2}) \geq \frac{1}{2} \lambda_{\min}^{1/2}(\Sigma_2 \Sigma_1).$$

Combining these facts with (24), we get

$$\|\hat{A} - A\| \lesssim \frac{\kappa(\Sigma_1)}{\lambda_{\min}^{1/2}(\Sigma_1 \Sigma_2)} \|E_2\| + \frac{\kappa(\Sigma_2) \|\Sigma_2\| \|\Sigma_1^{-1}\|}{\lambda_{\min}^{1/2}(\Sigma_2^{-1} \Sigma_1)} \|E_1\|. \quad (26)$$

Bounding $\|E_1\|$ and $\|E_2\|$. We apply now Theorem 2 in [37]. We obtain for any $t > 0$, with probability at least $1 - e^{-t}$,

$$\|E_1\| \leq C \|\Sigma_1\| \left(\sqrt{\frac{\mathbf{r}(\Sigma_1)}{n_1}} \vee \frac{\mathbf{r}(\Sigma_1)}{n_1} \vee \sqrt{\frac{t}{n_1}} \vee \frac{t}{n_1} \right),$$

and

$$\|E_2\| \leq C \|\Sigma_2\| \left(\sqrt{\frac{\mathbf{r}(\Sigma_2)}{n_2}} \vee \frac{\mathbf{r}(\Sigma_2)}{n_2} \vee \sqrt{\frac{t}{n_2}} \vee \frac{t}{n_2} \right),$$

for some sufficiently large numerical constant $C > 0$.

Taking $t_1 = 2 \log n_1$ and using condition (18), we obtain the result.

6.3 Proof of Theorem 1

Now lets go back to the original problem. We have

$$\|T(x) - \hat{T}(x)\| \leq \|m_2 - \hat{m}_2\| + \|A - \hat{A}\| \|x - m_1\| + \|\hat{A}\| \|\hat{m}_1 - m_1\| \quad (27)$$

Taking the expectation w.r.t. $x \sim \mu_1$, we get

$$\begin{aligned} \mathbb{E}_{x \sim \mu_1} \left[\|T(x) - \hat{T}(x)\| \right] &\leq \|m_2 - \hat{m}_2\| + \|A - \hat{A}\| \mathbb{E}_{x \sim \mu_1} [\|x - m_1\|] + \|\hat{A}\| \|\hat{m}_1 - m_1\| \\ &\leq \|m_2 - \hat{m}_2\| + \|A - \hat{A}\| \mathbb{E}_{x \sim \mu_1}^{1/2} [\|x - m_1\|^2] + \|\hat{A}\| \|\hat{m}_1 - m_1\|, \end{aligned} \quad (28)$$

where we use Cauchy-Schwarz's inequality in the last line.

Bounding $\mathbb{E}_{x \sim \mu_1}^{1/2} [\|x - m_1\|^2]$ is a straightforward computation. We get

$$\mathbb{E}_{x \sim \mu_1}^{1/2} [\|x - m_1\|^2] \leq C \|\Sigma_1\|^{1/2} \sqrt{\mathbf{r}(\Sigma_1)},$$

for some numerical constant $C > 0$.

Under conditions (5), (6) with Theorem 4, we get that

$$\|\hat{A}\| \leq_{\mathbb{P}} \|A\| + \|\hat{A} - A\| \leq C$$

for some numerical constant $C > 0$.

Combining (17), Theorem 4 with conditions (5), (6), we get with probability at least $1 - 3e^{-t} - \frac{1}{n_1}$,

$$d(T, \hat{T}) \leq C' \left(\sqrt{\frac{\mathbf{r}(\Sigma_2)}{n_2}} \vee \sqrt{\frac{\mathbf{r}(\Sigma_1)}{n_1}} \vee \sqrt{\frac{t}{n_1 \wedge n_2}} \vee \frac{t}{n_1 \wedge n_2} \right) \sqrt{\mathbf{r}(\Sigma_1)}, \quad (29)$$

for some absolute constant $C' > 0$. Up to a rescaling of the constant, we can replace probability $1 - 3e^{-t} - \frac{1}{n_1}$ by $1 - e^{-t} - \frac{1}{n_1}$.

7 Proof of theorem 2

In view of (11), we have

$$\begin{aligned} & \mathbb{E}_{(x,y) \sim \mathcal{P}_t} [L(y, f \circ \hat{T}^{-1}(x))] \\ &= \mathbb{E}_{(x,y) \sim \mathcal{P}_s} [L(y, f \circ \hat{T}^{-1}(T(x)))] \\ &= \mathbb{E}_{(x,y) \sim \mathcal{P}_s} [L(y, f \circ \hat{T}^{-1}(\hat{T}(x)))] + \mathbb{E}_{(x,y) \sim \mathcal{P}_s} [L(y, f \circ \hat{T}^{-1}(T(x))) - L(y, f \circ \hat{T}^{-1}(\hat{T}(x)))] \\ &\leq \mathbb{E}_{(x,y) \sim \mathcal{P}_s} [L(y, f(x))] + M_f M_L \mathbb{E}_{(x,y) \sim \mathcal{P}_s} [\|\hat{T}^{-1}(T(x)) - \hat{T}^{-1}(\hat{T}(x))\|] \quad (30) \\ &\leq \mathbb{E}_{(x,y) \sim \mathcal{P}_s} [L(y, f(x))] + M_f M_L \mathbb{E}_{(x,y) \sim \mathcal{P}_s} [\|\hat{A}^{-1}(T(x) - \hat{T}(x))\|] \\ &\leq R_s(f) + M_f M_L \mathbb{E}_{(x,y) \sim \mathcal{P}_s} [\|\hat{A}^{-1}\| \|T(x) - \hat{T}(x)\|] \\ &\leq R_s(f) + M_f M_L \|\hat{A}^{-1}\| d(T, \hat{T}), \quad (31) \end{aligned}$$

where the last two lines follows from the definition of \hat{T}^{-1} .

8 Proof of theorem 3

Let \mathcal{H}_K be a reproducing kernel Hilbert space (RKHS) associated with a symmetric nonnegatively definite kernel $K : \mathbb{R}^d \times \mathbb{R}^d \rightarrow \mathbb{R}$ such that for any $x \in \mathbb{R}^d$, $K_x(\cdot) = K(\cdot, x) \in \mathcal{H}_K$ and $f(x) = \langle f, K_x \rangle_{\mathcal{H}_K}$ for all $f \in \mathcal{H}_K$. See the seminal paper [38] for more details. Let Π_s be the marginal distribution of X^s and T_K be the integral operator from $L_2(\Pi_s)$ into $L_2(\Pi_s)$ with square integrable kernel K . Then it is known that the operator T_K is compact, self-adjoint and its spectrum is discrete. Let $\{\lambda_k\}_{k \geq 1}$ be the eigenvalues of T_K arranged in decreasing order and $\{\phi_k\}$ are the corresponding $L_2(\Pi_s)$ -orthonormal eigenfunctions. Then the RKHS-norm of any function f in the linear span of $\{\phi_k\}$ can be written as

$$\|f\|_{\mathcal{H}_K}^2 = \sum_{k \geq 1} \frac{|\langle f, \phi_k \rangle_{L_2(\Pi_s)}|^2}{\lambda_k}.$$

Set $f_*^s = \operatorname{argmin}_f R_s(f)$. Assume that $f_* \in \mathcal{H}_K$ and $\|f_*\|_{\mathcal{H}_K} \leq 1$. We consider the following empirical risk minimization estimator:

$$\hat{f}_{n_l} := \operatorname{argmin}_{\|f\|_{\mathcal{H}_K} \leq 1} \frac{1}{n_l} \sum_{i=1}^{n_l} l(Y_i^l, f(X_i^l)). \quad (32)$$

The performances of this procedure have been investigated in [27]. If we assume in particular that $\lambda_k \asymp k^{-2\beta}$ for some $\beta > 1/2$, then there exists a constant $C > 0$ such that with probability at least $1 - e^{-t}$,

$$R_s(\hat{f}_n) \leq R_s(f_*^s) + C \left(n_l^{-2\beta/(1+2\beta)} + \frac{t}{n_l} \right)$$

Under the assumptions of Theorem 1, we have $\|\widehat{A}^{-1}\| \leq_{\mathbb{P}} C$ for some numerical constant. Combining the previous display with (31) and Theorem 1, we get with probability at least $1 - e^{-t} - \frac{1}{n_1}$,

$$\begin{aligned}
R_t(\hat{f}_{n_l} \circ \hat{T}^{-1}) - R_s(f_*^s) &\lesssim n_l^{-2\beta/(1+2\beta)} + \frac{t}{n_l} \\
&\quad + M_f M_L \left(\sqrt{\frac{\mathbf{r}(\Sigma_2)}{n_2}} \vee \sqrt{\frac{\mathbf{r}(\Sigma_1)}{n_1}} \vee \sqrt{\frac{t}{n_1 \wedge n_2}} \vee \frac{t}{n_1 \wedge n_2} \right) \sqrt{\mathbf{r}(\Sigma_1)}.
\end{aligned} \tag{33}$$

The final bound use the fact that with our assumption $R_s(f_*^s) = R_t(f_*^t)$.